RSC Advances

ROYAL SOCIETY OF CHEMISTRY

PAPER

View Article Online
View Journal | View Issue



Cite this: *RSC Adv.*, 2025, **15**, 49501

# Sustainable recovery of high-purity nickel from real electroplating sludge *via* optimized leaching–precipitation process

The Anh Luu, Ai Quynh Nguyen, Van Doan Nguyen and Van Giang Le *

Received 7th November 2025
Accepted 7th December 2025

DOI: 10.1039/d5ra08573j

rsc.li/rsc-advances

This study presents an integrated process combining inorganic acid leaching and metal precipitation to recover nickel from real electroplating sludge, offering a sustainable approach suitable for direct application in production facilities in Vietnam. The leaching step was optimized using 5% $H_2SO_4$ at a solid/liquid (S/L) ratio of 1 : 10, a temperature of 55 °C, and a duration of 40 min, achieving a Ni leaching efficiency of 99.70% while also enabling the effective dissolution of Fe and other coexisting metals, thus demonstrating the high overall leaching efficiency of the process. The resulting leachate was subsequently treated with NaOH to precipitate nickel, with key parameters including pH (2–11), and initial $[Ni]_0$ concentration (500–4000 mg $L^{-1}$) systematically examined. Optimal conditions were identified at pH 9, and an initial $[Ni]_0$ concentration of 2000 mg $L^{-1}$, yielding a recovery efficiency greater than 98%. XRD analysis confirmed that the precipitate consisted predominantly of crystalline NiOOH and $Ni(OH)_2$ with negligible impurity phases. SEM images revealed uniform polyhedral crystals, and EDX spectra verified nickel as the dominant element with minimal contaminants. Collectively, these findings demonstrate that the proposed process delivers both outstanding metal recovery and minimal secondary pollution, providing an economical, environmentally benign, and practical solution for small-scale industrial treatment of electroplating sludge.



## 1. Introduction

Electroplating sludge (EPS), a byproduct generated during the treatment of wastewater containing heavy metals, is classified as hazardous waste under the regulations of many countries including Vietnam.[1,2] EPS typically contains metals such as Cu, Ni, Zn, Fe, and Cr, which exist in the form of hydroxides or oxides within a complex mixture of solids and liquids, accompanied by high moisture content (35–92%) and impurities like Fe, Al, Si, Ca, Mg, and Na.[3,4] Some of these metals are present at high concentrations and are toxic even at low levels, increasing the risk of soil and groundwater contamination as well as bioaccumulation in the food chain if not treated properly.[5,6] Consuming food contaminated with heavy metals has been shown to cause immunosuppression, reduced fertility, and acute poisoning when concentrations are high.[7]

Historically, electroplating sludge has been managed through landfilling or solidification to isolate toxic components,[8] but these methods are increasingly being reconsidered due to environmental concerns and the growing recognition of EPS as a secondary source of valuable metals. In Vietnam, most of the sludge from nickel plating operations is currently treated using traditional physicochemical methods, which do not fully exploit the valuable metals present in the waste. Alternative metal recovery approaches, including ion exchange, membrane filtration, electrochemical techniques, and the use of organic solvents have been proposed but still face several limitations such as low recovery efficiency, high operational costs, or incompatibility with actual industrial conditions in the country.[9,10] Some research has demonstrated that organic solvents like α-hydroxy sulfonic acid, prop-2-enoic acid, or decanoic acid can effectively dissolve metals such as Zn, but their effectiveness is limited by dilution effects due to water in the sludge.[11]

Recent trends have therefore shifted towards processes that not only stabilize toxic constituents but also enable the separation and recovery of metals such as nickel and iron.[12] Among the available methods, chemical precipitation, which is traditionally applied for metal removal in wastewater treatment, is now being repurposed as a practical and cost-effective method for recovering valuable metals from EPS in the form of solid precipitates.[13] This technique primarily depends on the use of inorganic or organic acids to dissolve metals.[14] For example, Ahmadabad-based studies demonstrated that ferric phosphate can be cleanly precipitated from acid-leached electroplating sludge at ambient temperature (20 °C, pH 1.5–2.0), followed by nickel recovery reaching 98.7% yield after separation from Fe and Cr.[15] In another approach, nickel hydroxide can be precipitated from mixed-metal leachate by adjusting pH to 9

*Central Institute for Natural Resources and Environmental Studies, Vietnam National University, Hanoi 100000, Vietnam. E-mail: levangiangcres@vnu.edu.vn*

using NaOH, achieving over 85% Ni recovery with high purity.[16] Other research has demonstrated that stepwise adjustment of pH (*e.g.*, precipitating Fe(III) at pH 3–4 while keeping Ni(II) in solution) enables selective recovery, further tuning using chelating agents or controlling ionic strength can bolster selectivity and reduce co-precipitation of impurities.[17]

To address these challenges, this study proposes an integrated approach combining acid leaching and chemical precipitation to separate and recover nickel and iron from real electroplating sludge under conditions that reflect the operational realities of electroplating facilities in Vietnam. The research focuses on evaluating how the initial physical properties of the sludge, particularly water content and particle size, affect the leaching efficiency. It also investigates the performance of the separation system by analyzing the influence of several key parameters, including the concentration and ratio of inorganic acids, as well as factors such as reaction time, temperature, stirring speed, and the S/L ratio. Following leaching, the present work systematically examines how precipitation pH (ranging from 2 to 11) and the initial nickel concentration (500–4000 mg $L^{-1}$) influence metal recovery efficiency and impurity removal. The solid phase obtained from the precipitation process was analyzed to determine the crystalline phases, surface functional groups, and elemental composition of nickel, iron, and accompanying elements using XRD and SEM-EDX. The novelty of this work lies in its focus on real sludge from industrial sources and in the optimization of precipitation conditions to achieve high metal recovery efficiency while minimizing impurity contamination. The proposed process is designed to be environmentally sustainable, economically viable, and adaptable for small-scale application directly within industrial production facilities.

## 2. Experimental

### 2.1. Materials

The nickel-containing sludge sample used in this study was collected from the Binh Nguyen Environmental Development Joint Stock Company, located in Phu Lang Commune, Que Vo District, Bac Ninh Province. The sample originated from the electroplating wastewater treatment process. After collection, visible stones and organic debris were removed. The sludge was then dried at 105 °C for 2.5 h and gently crushed to obtain a homogeneous powder. The prepared samples were properly sealed and stored under controlled conditions to preserve their integrity for subsequent analyses. The XRD spectrum of the original Ni-containing sludge is shown in Fig. S1, while the elemental composition of the sludge is summarized in Table S1. Broad diffraction bands characteristic of an amorphous structure are observed, along with several weak peaks that may correspond to $CaCO_3$ and $CaSO_4$. No distinct diffraction peaks of crystalline metal compounds were detected, suggesting that metal elements such as Ni are predominantly present in amorphous forms (*e.g.*, $Ni(OH)_2$, $Fe(OH)_3$, $Al(OH)_3$), which are difficult to identify clearly by XRD.

Prior to the leaching experiments, 0.25 g of the dried sludge was digested in a mixture of concentrated $HNO_3$ and HCl using a microwave-assisted acid digestion procedure (Milestone ETHOS UP, 1900 W maximum power) equipped with PTFE-TFM vessels (100 mL capacity, maximum pressure 100 bar). The digestion was performed at 180 °C and 40 bar for 90 min (15 min ramp and 75 min hold). The digestate was filtered through a 0.45 μm membrane and analyzed by inductively coupled plasma mass spectrometry (ICP-MS, Thermo Fisher Scientific). Metal standards (1000 mg $L^{-1}$, 23 elements) were used for calibration and deionized water with resistivity >18.2 MΩ cm was used throughout. The overall experimental procedure for acidification, filtration, and ICP measurement is illustrated in Fig. S2, while the sludge samples before and after digestion, as well as the digestate solution are shown in Fig. S3.

Water content and particle size distribution were investigated by drying pre-weighed containers and sludge samples at various temperatures (room temperature, 70 °C, 105 °C, and 150 °C) with time intervals ranging from 0.5 to 46.0 h. Each container and its lid were pre-dried at 105 °C for 2 h and cooled in a desiccator for at least 45 min before weighing. A set of sludge samples with targeted water levels (5%, 10%, 20%, 30%, and 40%) was then prepared for leaching experiments to identify the optimal water content for maximum metal recovery. To assess the effect of particle size, dried sludge with the optimal water condition was ground and sieved into six fractions: <0.15 mm, 0.15–425 mm, 0.425–1.18 mm, 1.18–2.0 mm, and 2.0–5.6 mm. Each 50 g sludge sample was leached with 5% HCl at a S/L ratio of 1 : 10 for 1 h under magnetic stirring at 200 rpm and ambient temperature. For inorganic acid digestion, experiments were carried out using different acids, including $H_3PO_4$, HCl, $HNO_3$, and $H_2SO_4$ at concentrations ranging from 5% to 20%. The experiments were conducted for 1 h at room temperature with a S/L ratio of 1 : 15 and magnetic stirring at 200 rpm. Based on the most effective acid, the study further assessed the performance of the influence of the S/L ratio was investigated at values of 1 : 5, 1 : 8, 1 : 10, 1 : 12, and 1 : 15. The effects of temperature and reaction time were systematically studied at 45, 55, 65, and 75 °C, with sampling at 15, 30, 45, 60, 75, 90, and 120 min. After each experiment, the leachate was acidified to prevent precipitation before metal concentration analysis. Following leaching optimization, a precipitation process was performed for the recovery of nickel from the leachate. The pH of the filtrate was adjusted by dropwise addition of NaOH solution under continuous magnetic stirring at 250 rpm. The initial nickel concentration in the solution was adjusted between 500 and 4000 mg $L^{-1}$. The precipitates were subsequently characterized to determine phase composition and nickel recovery efficiency. Each experimental step including leaching and precipitation was repeated three times to verify the reproducibility of the data.

### 2.2. Reagents and chemicals

Chemicals including hydrochloric acid (HCl, 36%), nitric acid ($HNO_3$, 65%), sulfuric acid ($H_2SO_4$, 98%), phosphoric acid ($H_3PO_4$, 99%), and sodium hydroxide (NaOH, 99%) were all of analytical grade and obtained from Merck or equivalent suppliers. Ultrasonic cleaning baths, magnetic stirrers (AREX

 

Digital, Velp), drying ovens, and sieving equipment were used to support solid preparation, metal leaching, and moisture control. All analytical procedures and metal quantification were carried out at the Laboratory of Environmental Resources and Analysis, Vietnam National University, Hanoi, which is certified under Vimcerts 327 by the Ministry of Natural Resources and Environment.

### 2.3. Analytical methods

The pH values were manually determined using a portable meter (model TS-110, Suntex, Taiwan). The quantification of metal elements was conducted *via* inductively coupled plasma mass spectrometry (ICP-MS), using the iCAP RQ instrument from Thermo Fisher Scientific. For ammonium ($NH_4^+$) and phosphate ($PO_4^{3-}$) concentration measurements in both influent and effluent samples, analyses were performed based on the SFS-EN ISO 6878 standard method employing a flow injection analyzer (FIA, Lachat Instruments 5600, Colorado, USA). The crystalline structure of the dried granules was characterized using X-ray diffraction (XRD), performed on a Rigaku RX III diffractometer (Japan). The scans were recorded using CuKα radiation (40 kV, 30 mA), ranging from 10° to 90°, with a step size of 0.05° and a dwell time of 0.5 seconds per step. The surface morphology of the granules was visualized *via* scanning electron microscopy (SEM) using a Hitachi SU8010 microscope (Japan). Prior to imaging, the samples were coated with a thin layer of platinum using a JFC-1600 sputter coater (JEOL). Additionally, an energy-dispersive spectrometer (EDX, LINKS AN10000/85S, Japan), attached to the SEM system, was employed to investigate the elemental composition and surface functional groups of the materials.

## 3. Results and discussions

### 3.1. Effect of drying temperature

The effect of drying temperature on the efficiency of water removal over time is depicted in Fig. S4. The data clearly show that higher temperatures lead to significantly faster and more complete water removal from the material. At 24 °C, the drying process is slow and incomplete with water removal reaching only 42.0% even after 24 h. In contrast, with this same time period at 70 °C, the sample reaches about 54.83% water loss and plateaus afterward. When the temperature increases further to 105 and 150 °C, the drying rate becomes almost instantaneous, achieving over 54% water removal in less than 2.5 h with no significant increase observed with longer drying time. The above behavior is consistent with fundamental drying theory, where higher temperatures increase the vapor pressure of water, enhance thermal conductivity, and reduce the relative humidity of the surrounding air, all of which promote faster evaporation.[18] Moreover, the steep drying curves at 105–150 °C indicate that the material primarily undergoes constant-rate drying at the beginning, followed by a rapid transition into the falling-rate period, in which bound water becomes dominant.[19] Although higher temperatures improve drying efficiency, the marginal gain between 105 and 150 °C is negligible, suggesting that temperatures above 105 °C may be thermally excessive, especially when considering energy consumption and potential changes in material structure. Therefore, a drying temperature of 105 °C may be considered optimal in balancing speed, efficiency, and thermal safety.

### 3.2. Effect of water content

The effect of water on the leaching efficiency of metals is shown in Fig. 1(a). The results indicate that the leaching efficiency decreases significantly as the sample water increases from 5% to 56%. At 5–12% water content, the leaching efficiency remained stable at 99.70% for Ni and 98.20% for Fe. Under the same conditions, Cr and Al also reached very high values, 92.79–98.85% and 95.0–96.10%, respectively, indicating almost complete solubility at low water content. Nonetheless, at 42.5% water content, the corresponding drops were to 56.50% and 66.05%, respectively, whereas Cr recorded a more pronounced decrease, dropped to 78.35% and Al reached 69.17% lower than both Ni and Fe, reflecting the greater sensitivity of aluminum to increased water content in the sample. Then, these values remained almost unchanged at 56% water with corresponding efficiencies of 55.80%, 59.67%, 51.86%, and 50.05%, respectively. The above trend clearly shows the hindering effect of

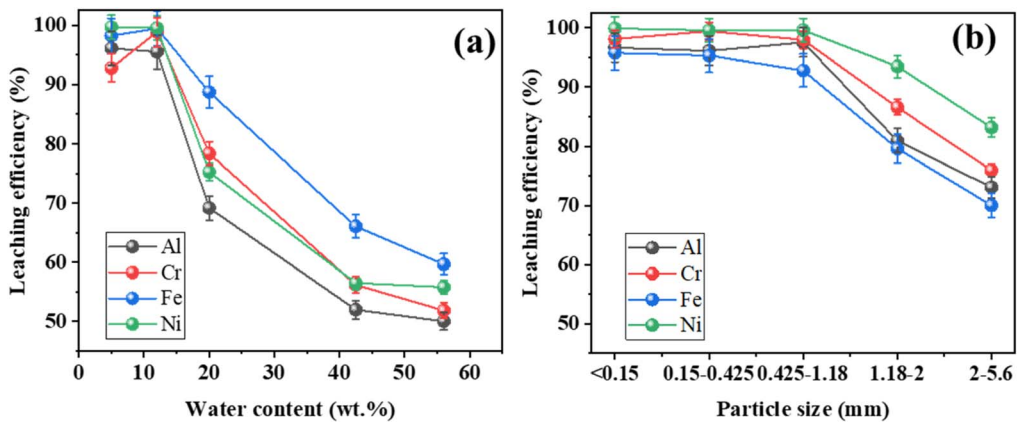


Fig. 1 Effect of (a) water content and (b) particle size on Ni, Fe, Cr, and Al leaching efficiency. Error bars indicate the standard deviation calculated from three replicates.

excess water in the reaction environment. At high water, excess water can dilute the leaching agent and reduce the concentration of protons or complexing species. This limits the effective contact between the solid and the leaching solution. Furthermore, water may slow the diffusion of metal ions from the solid to the liquid phase, especially in systems governed by diffusion mechanisms such as the shrinking-core model. Notably, while the efficiency loss for Fe was greater than that for Ni at almost water content levels, both Cr and Al also exhibited pronounced declines, with Al showing the lowest leaching efficiency overall, indicating that all four metals are strongly inhibited under high water content conditions.[20] The above result suggests that iron is more sensitive to humid conditions, possibly due to the formation of insoluble oxide layers or less favorable mineral structures. These findings highlight the importance of pretreatment steps, such as drying or dehumidifying the sample, to ensure high recovery rates in sludge or moist solid leaching processes.

### 3.3. Effect of particle size

Fig. 1(b) shows a clear trend that when the particle size decreases from about 2–5.6 mm to 0.15–0.425 mm, the Ni leaching efficiency rises significantly by approximately 17% and exceeds 95% at the smallest size. Specifically, particles of 0.15–0.425 mm achieve efficiencies of 99.62% while larger particles around 2–5.6 mm reach only 83.17%. Similarly, Cr and Al also exhibit improved efficiencies at finer sizes, reaching 99.45% and 96.12% at 0.15–0.425 mm, compared to 75.91% and 73.07% at 2–5.6 mm, respectively. This improvement is due to the increased specific surface area and faster reaction rate, which align with the shrinking core model and diffusion-controlled mechanisms. Parhi *et al.* (2013) also demonstrated that under leaching conditions of 323 K and 1 M HCl, nickel was almost completely dissolved (99.9%) within two hours, while the co-dissolution of aluminum was limited to about 1%.[21] Meanwhile, iron is the least sensitive to particle size, yet still benefits from size reduction, achieving 95.78% separation at 0.15–0.425 mm and falling to 70.01% in the coarsest fraction (2–5.6 mm). A comparable decreasing trend was also observed for Cr and Al, which although exhibiting higher extraction efficiencies at finer particle sizes, experienced substantial declines in the coarse fraction. The aforementioned trend is consistent with diffusion-controlled shrinking-core mechanisms previously reported for iron oxides in fine particles, and highlights the significant influence of particle size on nickel dissolution behavior.[22,23] These results indicate that reducing particle size significantly enhances the overall leaching efficiency. However, further decreasing the particle size below 0.15 mm, despite providing slightly higher dissolution rates, would require substantially greater energy input during grinding. Therefore, a particle size range of 0.15–0.425 mm was selected as an optimal balance between leaching efficiency and energy consumption.

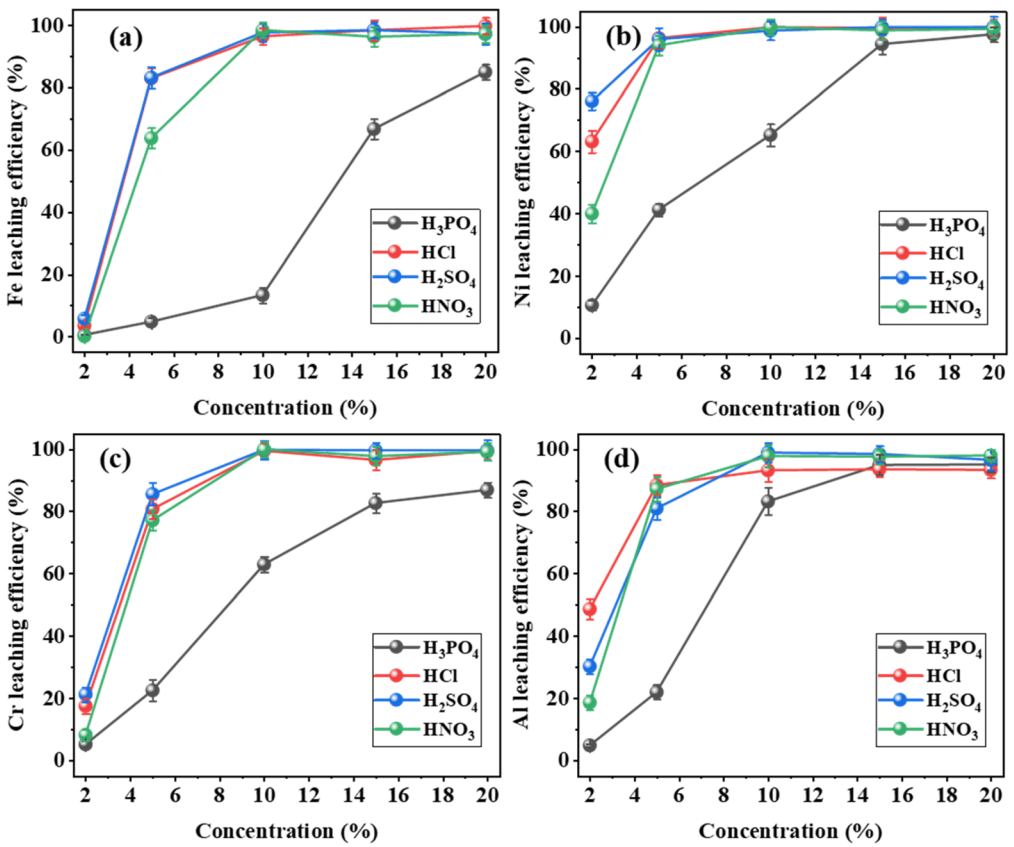


Fig. 2 Effect of (a–d) concentration of acid on the metals leaching efficiency. Error bars indicate the standard deviation calculated from three replicates.

### 3.4. Effect of various acidifying agents

The results presented in Fig. 2(a–d) show a clear effect of acid concentration on the leaching efficiency of Fe, Ni, Cr, and Al metals in electoplating sludge under the investigated conditions of 60 min, S/L of 1/15, and stirring speed 200 rpm. In Fig. 2(a), the Fe leaching efficiency increases rapidly when the acid concentration increases from 2% to 8%, especially when using strong acids such as HCl, $H_2SO_4$, and $HNO_3$. Notably, the efficiency reaches over 95% at a concentration of 10% and almost completely (>98%) at 12% or higher. In contrast, the leaching efficiency with $H_3PO_4$ was only about 84.87% even at 20% acid concentration, clearly indicating that the weak acidity and low dissociation capacity of $H_3PO_4$ are insufficient to provide the amount of $H^+$ ions needed to break the Fe oxide lattice structure. This mechanism is consistent with previous work on iron oxide dissolution with phosphoric acid, which showed limited dissolution under moderate conditions.[24] In contrast, $H_2SO_4$ only reached 46.12% under the same conditions, emphasizing the role of acid strength and complexation ability in the leaching of base metals such as Fe and Al. Meanwhile, Fig. 2(b) illustrates the leaching yield of Ni, which exhibits a similar increasing trend and reaches an optimal value at a 10% acid concentration when using strong acids. Specifically, HCl, $H_2SO_4$, and $HNO_3$ achieved yields of 99.90%, 98.76%, and 99.91%, respectively, whereas $H_3PO_4$ only reached approximately 65.24% even at a concentration of 10%. The higher leaching yield of Ni compared to Fe under identical conditions indicates its greater chemical reactivity in acidic media and is further supported by previous findings. Specifically, Ali *et al.* (2023)[25] reported that leaching Ni from abraded nickel alloy using 3 M HCl resulted in nearly 100% yield after 60 min at 100 °C, following the 'shrinking core' model in which diffusion through the solid product layer controls the reaction rate.

The results in Fig. 2(c) demonstrate that Cr leaching efficiency is strongly dependent on acid concentration, with both the trend and absolute values varying markedly among the acids tested. At 2% concentration, the efficiency remains very low, reaching only 4.67% with $H_3PO_4$, 18.50% with $HNO_3$, 30.15% with $H_2SO_4$, and 48.58% with HCl. Increasing the concentration to 5% causes a sharp rise in the metal leaching with HCl 88.49%, $H_2SO_4$ 80.99%, and $HNO_3$ 87.23% whereas $H_3PO_4$ reaches only 21.87%. At double or higher concentrations, Cr is almost completely leached by HCl, $H_2SO_4$, and $HNO_3$ (all above 93%), while $H_3PO_4$ plateaus at about 83.23%. These disparities reflect differences in acid strength and $H^+$ dissociation capacity: strong acids generate high proton activity that can break the stable $Cr_2O_3$ lattice and release $Cr^{3+}$ into solution, especially under agitation, whereas $H_3PO_4$ as a weak acid has limited dissociation and thus insufficient proton supply to attack $Cr_2O_3$ effectively. This mechanistic interpretation is supported by broader reviews of hydrometallurgical extraction, which emphasize that stronger inorganic acids more effectively solubilize metal oxides and overcome thermodynamic stability barriers.[26] Furthermore, $Cr_2O_3$ is known for its high thermal and chemical stability under acidic environments,[27] so only sufficiently strong acid environments can efficiently dissolve it.

As illustrated in Fig. 2(d), aluminum exhibits higher leaching efficiency than chromium, with both metals showing enhanced dissolution under stronger acidic conditions. At a concentration of 2%, the Al leaching efficiency remains low with values of 4.67% for $H_3PO_4$, 18.50% for $HNO_3$, 30.15% for $H_2SO_4$, and 48.58% for HCl. When the concentration increases to 5%, these value rises sharply to 88.49%, 80.99%, and 87.23%, respectively, whereas $H_3PO_4$ is still limited to 21.87%. At concentrations doubled or higher, the Al removal with strong acids is nearly complete with HCl reaching 93.27% to 93.58%, $H_2SO_4$ reaching 96.64% to 98.96% and $HNO_3$ reaching 97.65% to 98.02%, whereas $H_3PO_4$ achieves only 83.23% at 10% and approaches 95.12% at 20%. The above behavior reflects the amphoteric character of $Al_2O_3$, whose crystal lattice is readily attacked by protons in a strong acidic environment, which facilitates the release of $Al^{3+}$ ions into solution. The presence of $Cl^-$, $SO_4^{2-}$, and $NO_3^-$ anions also promotes the formation of stable aqueous complexes with $Al^{3+}$ that stabilize the dissolved species and enhance the overall leaching process as reported in previous studies of aluminum dissolution in mineral acids.[28] This is consistent with the research results of Jha *et al.*,[29] who showed that HCl and $H_2SO_4$ are effective solvents for separating Al from metallurgical sludge, thanks to the combined mechanism of protonation and ion complexation in solution. In addition, the solution (diluted 100 times) after leaching with $H_2SO_4$ at concentrations of 2 – 5 – 10 – 15 – 20% is depicted in Fig. S5.

Taken together, the results indicate that acid concentration is a key parameter governing the leaching efficiency, especially for transition metals. Strong acids such as HCl, $H_2SO_4$, and $HNO_3$ demonstrate high extraction efficiency at concentrations of 10% while $H_3PO_4$ remains considerably less effective across all tested levels. It should be noted that using highly concentrated acids is not preferred when developing large-scale metal recovery processes. Such acid solution concentrations can lead to significant corrosion of equipment that comes into direct contact with the acid, necessitating frequent maintenance or replacement. Moreover, the leaching process may be further complicated by the release of metal impurities, thereby affecting the efficiency of downstream filtration.[30,31] In efforts to optimize the leaching process for metal recovery from electroplating sludge, $H_2SO_4$ at a concentration of 5% was selected as the primary leaching reagent, owing to its high extraction efficiency for key metals such as iron (Fe) and nickel (Ni). These findings align with those reported by Kurniawan *et al.*, who identified $H_2SO_4$ as an effective and cost-efficient agent for leaching heavy metals from electrochemical waste materials.[32] Intending to develop a cost-effective process for Ni recovery, this study prioritized the use of common dilute acids rather than expensive or highly concentrated alternatives from the outset.

### 3.5. Effect of S/L ratio

The ratio between the mass of electroplating sludge and the volume of acid solution significantly influences metal leaching efficiency. As shown in Fig. 3(a), increasing the S/L ratio from 1 : 5 to 1 : 8 results in a sharp improvement in the leaching

efficiency. Specifically, the recovery of Fe increased from 35.30% to 94.33%, while that of Ni rose from 74.93% to 98.96%. In contrast, the separation efficiencies of Al and Cr exhibited a more pronounced improvement, increasing sharply from 55.6% and 51.0% at an S/L ratio of 1/5 to above 93% when the ratio was reduced to 1/8–1/10, beyond which the values tended to stabilize. With further increases in acid volume, the leaching efficiencies of Fe and Ni reach a plateau and remain relatively unchanged. The limited enhancement observed at higher S/L ratios is mainly due to the insufficient concentration of $H^+$ ions, which play a crucial role in dissolving metal oxyhydroxides, the primary components of electroplating sludge.[33] Moreover, a low solution volume restricts the diffusion of metal ions from the sludge surface, reducing the completeness of the separation process. Under these conditions, the local pH may also increase due to the dissolution of products, which inhibits complex formation and the breakdown of the protective oxyhydroxide layer on iron and nickel. In contrast, a larger acid volume ensures an acidic environment with an abundance of $H^+$ ions, which accelerates the dissolution reaction.[34] The dissolution reaction mechanism follows the "shrinking-core" model and is governed by the diffusion rate through the solid product layer, as summarized in the overview studies on metal leaching kinetics[33] and experimental applications in laterite ore.[35] Recent

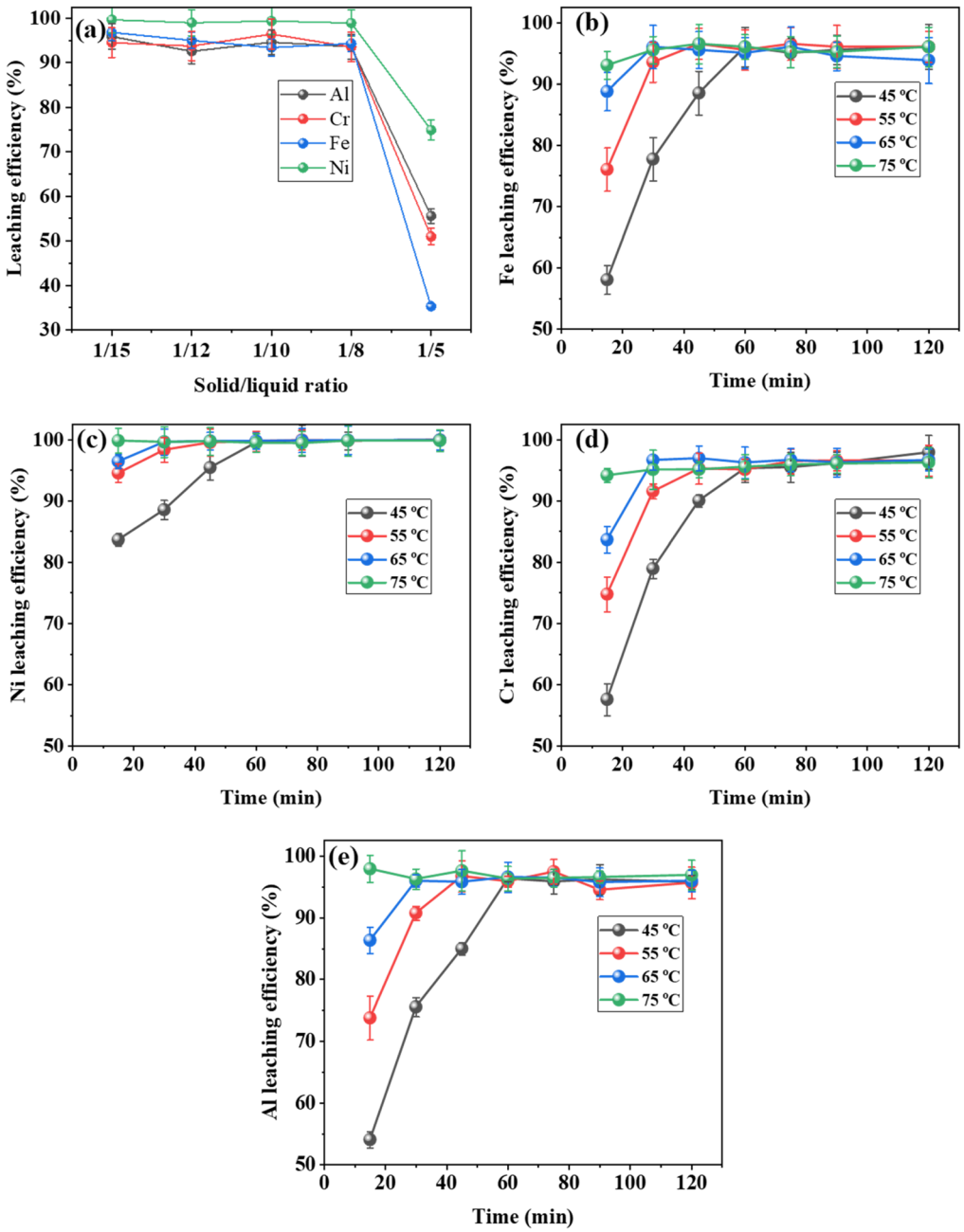


Fig. 3 Effect of (a) S/L ratios and (b–e) temperature and duration time on the leaching efficiency. Error bars indicate the standard deviation calculated from three replicates.

studies such as Ibrahim *et al.*[36] also confirmed that the optimum Ni extraction efficiency was obtained at 45–60 min and S/L around 1/10, while excessive time or high S/L resulted in a decrease in reaction efficiency due to product membrane regeneration. Furthermore, a specific study on Morowali laterite ore (Li *et al.* 2022) noted that with decreasing S/L and increasing time, Ni yield increased but exceeding 60 min or high S/L (*i.e.*, too much solid) would reduce yield due to slow diffusion rate and lack of protons in the solution.[37] These results indicate that a leaching time of 60 min combined with an S/L ratio of 1/8–1/10 provides the optimal condition for metal extraction from wastewater sludge using mixed acids, thereby offering valuable guidance for the design of efficient and sustainable industrial recovery processes.[38]

### 3.6. Effect of reaction time and temperature

Reaction time and temperature are critical factors that directly influence metal leaching efficiency in solid–liquid systems. As depicted in Fig. 3(b), the leaching efficiency of Fe increases progressively with both reaction time and temperature, particularly evident during the initial phase. At 45 °C, which corresponds to typical room-temperature stirring conditions, Fe leaching reaches 58.50% after 15 min and rises to 96.10% after 60 min. Beyond 60 min, the increase in efficiency is minimal, indicating that prolonged time has a limited additional effect. This behavior suggests that most of the kinetically accessible Fe species are rapidly solubilized during the early stage, while the remaining fraction is either strongly bound within the solid matrix or controlled by slower diffusion processes through the pores.[39,40] The obtained results suggest that the reaction does proceed, but at a relatively slow rate, which is consistent with a transition from a chemically controlled regime to a diffusion-limited regime as the leaching progresses.[41] When the temperature was raised to 55 °C, Fe recovery remained modest at 76.10% after 15 min but exceeded 96% at 60 min, underscoring the crucial role of thermal activation in accelerating both the complexation between Fe ions and the leaching agents and the mass transfer across the solid–liquid interface. At higher temperatures of 65 °C and 75 °C, Fe leaching reaches over 95% after just 30 min and remains nearly constant thereafter. This plateau suggests that equilibrium is quickly established, and further increase in time contributes little to leaching efficiency.[42] However, even at 75 °C, the maximum efficiency does not exceed 96.5%, implying that a portion of Fe may be bound in insoluble forms such as phosphates or oxalates, which restrict complete leaching. Based on these results, 65 °C appears to be an optimal temperature, balancing high efficiency with reasonable energy consumption, while also ensuring that kinetic limitations are sufficiently overcome without excessive thermal input.

In contrast, the leaching behavior of Ni is significantly more favorable under all tested conditions (Fig. 3(c)). At 45 °C, Ni recovery reached 95.42% after 45 min and further improved to 99.64% at 60 min. When the temperature was raised to 55 °C, the recovery exceeded 99% within 45 min. A subsequent rise of 10–20 °C accelerated the process even more, yielding 99.71–99.90% dissolution within 30–60 min and confirming the rapid and nearly complete leaching of Ni. This notable difference between Ni and Fe may arise from the higher susceptibility of Ni compounds in plating sludge to protonation or complexation while Fe tends to form less soluble salts that inhibit dissolution,[43] as observed in ultrasonic sulfuric acid leaching of nickel residues, where Ni leaching was diffusion-controlled through the product layer at lower temperature but rate increased steeply with temperature.[44] For Cr and Al, the results in Fig. 3(d and e) show that the dissolution efficiency depends strongly on both reaction time and temperature. At 45 °C, Cr reaches only about 42.12% after 15 min and gradually increases to 92.34% after 60 min. When the temperature is raised to 55 °C, the efficiency reaches 70.54% at 15 min and nearly 97% after 60 min. At 65 °C and 75 °C, Cr exceeds 95% within 30 min and stabilizes at nearly 98% by the end of the experiment. These observations suggest that stable $Cr^{3+}$ phases or insoluble oxide or hydroxide layers may slow proton diffusion and surface reactions, which similar to findings on $Cr(OH)_3$ oxidation and dissolution kinetics where diffusion through the oxide/hydroxide barrier is rate-limiting.[45] Aluminum follows a similar pattern but dissolves more slowly at lower temperatures. At 45 °C, the yield is about 25.08% after 15 min and increases to 84.65% after 60 min. When the temperature is raised to 55 °C, the yield reaches 60.63% at 15 min and exceeds 90% after 60 min. At 65 °C and 75 °C, Al dissolves rapidly, reaching more than 95% within 30 min and remaining nearly constant until the end of the reaction. The pronounced increase in yield with increasing temperature confirms that diffusion through the product layer, such as $Al(OH)_3$ or Al-oxalate, is the rate-limiting step and that this process is strongly enhanced as the solution viscosity and increased diffusion coefficient, analogous to kinetic acid leaching studies where temperature rise reduces the resistance of the diffusion barrier and accelerates metal dissolution.[44] In addition, the correlation between temperature and leaching efficiency at 15 min was also constructed to further clarify the metal dissolution behavior in the early stage, and these correlation graphs are presented in Fig. S6. The leaching process in this system is a heterogeneous reaction that occurs at the interface between the solid samples and the acid solution. It typically involves three main steps: (i) diffusion of protons ($H^+$ ions) toward the solid surface, (ii) a chemical reaction at the interface between the acid and the metal species, and (iii) diffusion of reaction products away from the solid–liquid boundary layer. An increase in temperature enhances the kinetic energy of the molecules, thereby increasing the frequency and effectiveness of collisions between $H^+$ ions and the solid surface. This promotes faster reaction rates. The relationship between temperature and reaction rate can be quantitatively described by the Arrhenius equation:[46]

$$K = Ae^{-E_a/(RT)} \quad (1)$$

In which: $K$ is the reaction rate constant, $A$: Arrhenius coefficient, $E_a$: activation energy, $R$: gas constant, and $T$: absolute temperature.

In addition, elevated temperatures reduce the viscosity of the solution and enhance the diffusion coefficient, thereby facilitating the mass transport of hydrogen and metal ions in the liquid phase.[47] This effect is particularly significant in electroplating sludge systems, where diffusion through the surface product layer, such as insoluble oxides or salts, often constitutes the primary rate-limiting step in the leaching process. However, when the temperature exceeds the optimal range, undesirable side reactions may occur, including the oxidation of ferrous ions ($Fe^{2+}$) to ferric ions ($Fe^{3+}$), which are substantially less soluble in acidic media.[48] Accordingly, selecting an appropriate temperature is crucial not only for accelerating reaction kinetics but also for enhancing metal recovery efficiency and minimizing adverse effects on the chemical system and processing equipment. This observation aligns with previous findings, whereas Hidayat *et al.*[49] reported that the leaching efficiency of nickel increased rapidly within the first 30 to 60 min and gradually reached a steady state thereafter. These results suggest that the leaching process approached a dynamic equilibrium after approximately 30 min at 65 °C, at which point the solubility of the metals had nearly reached its maximum under the experimental conditions.

## 4. Precipitation performance evaluation

### 4.1. Effect of pH

The results of metal recovery as precipitates demonstrate that pH is a decisive parameter for both selective separation efficiency and the kinetic mechanism of the process (Fig. 4(a–d)). In the low pH range (2–4), Fe, Al, and Cr were readily solubilized but subsequently precipitated due to the high solubility and rapid supersaturation of their hydroxides. A sharp increase in recovery was observed as the pH rose from 2.0 to 4.0, with Fe, Al, and Cr recoveries improving from 43.0%, 15.9%, and 17.2% to nearly 100%, 89%, and 65%, respectively. In contrast, Ni predominantly persists in solution as stable $Ni^{2+}$ ions, and its recovery remains negligible in this region, only 13.9–19.4%. When the pH increases to about 5–6, Fe and Al precipitate completely (100% recovery) while Cr also exceeds 94%, thereby removing most of these metals from solution. At the same pH, the recovery of Ni remains relatively low with only 24.2% at pH 4.5 and 46.4% at pH 6, because the saturation threshold required for hydroxide precipitation has not yet been reached. In the pH 4–6 range, Fe, Al, and Cr are fully precipitated as their respective hydroxides, which possess extremely low solubility. The resulting inorganic sludge is subsequently collected, thickened, and subjected to appropriate stabilization/solidification treatments to ensure environmental safety. Owing to the strong immobilization capacity of Fe–Al–Cr hydroxide matrices, the re-dissolution of metal ions is effectively prevented, minimizing the risk of secondary contamination. Additionally, depending on process conditions, this sludge stream may be considered for reuse as a Fe–Al-rich auxiliary raw material source. The clarified supernatant at this stage contained mainly sulfate species with negligible dissolved metals, indicating that after proper pH adjustment it could be reused as the extraction medium in subsequent cycles, thereby reducing fresh acid/alkali consumption and wastewater generation. Although impurity accumulation and long-term stability were not assessed in this study, future work should examine how recirculation influences proton availability, metal dissolution kinetics, and overall process efficiency. Subsequently, nucleation and crystal growth of Ni occur only at pH $\geq$ 7.5, where its recovery sharply rises to 84.6% and then approaches 100% at pH $\geq$ 9 in the form of pure $Ni(OH)_2$. This is consistent with the very small solubility product constant of $Ni(OH)_2$ ($K_{sp} \approx 2.0 \times 10^{-15}$ at 25 °C).[50] The precipitation process can be divided into three main stages: (i) solution supersaturation when the $OH^-$ concentration becomes sufficiently high, (ii) nucleation through the formation of amorphous $Ni(OH)_2$ clusters, and (iii) subsequent crystal growth until a steady state is reached. In addition, co-precipitation of Ni with Fe and Al hydroxides, which precipitate at lower pH values, may occur and significantly influence both the precipitation kinetics and the purity of the final product. These observations are consistent with previous reports. Mubarok (2013) obtained Ni yields up to

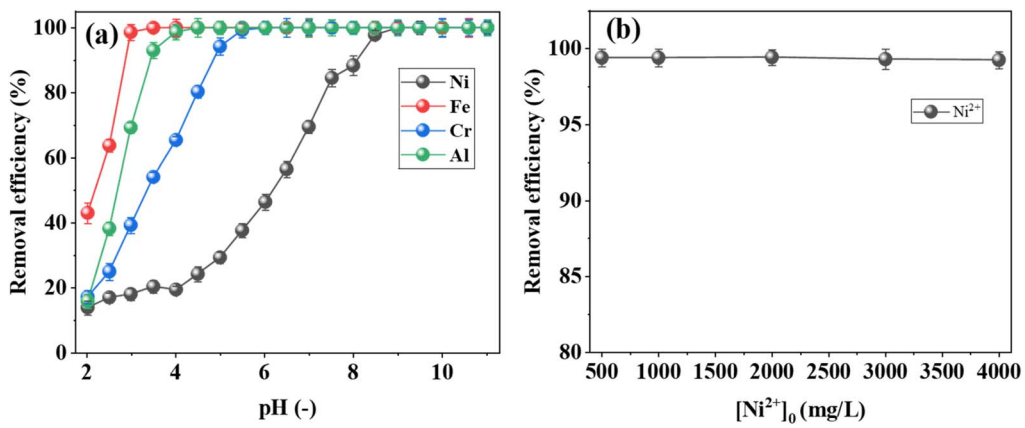


Fig. 4 Effect of (a) pH (–) and (b) $[Ni^{2+}]_0$ concentration on the nickel precipitation. Error bars indicate the standard deviation calculated from three replicates.

99.9% at pH 9 in a sulfate medium.[51] Sist and Demopoulos (2010) highlighted the role of supersaturation and stirring speed in controlling nucleation and the growth kinetics of $Ni(OH)_2$.[52] Mavis (2003) showed that longer digestion times allowed amorphous $Ni(OH)_2$ to transform into stable β-$Ni(OH)_2$ crystals, thereby improving both purity and filterability.[53] More recently, Shekarian *et al.* (2025) demonstrated that optimal precipitation of Ni requires a higher pH than other metal species, typically within 9–10.5, and emphasized kinetic control through alkali addition rate and agitation conditions to minimize impurity co-precipitation.[54] Thus, the present findings not only align with international research trends but also clarify the nucleation-growth mechanism and the crucial role of supersaturation in achieving pure Ni recovery. These insights open up opportunities to optimize multi-stage precipitation technology for the treatment of electroplating sludge.

### 4.2. Effect of initial $[Ni^{2+}]_0$

The effect of the initial $[Ni^{2+}]_0$ concentration in the range of 500–4000 mg $L^{-1}$ was investigated, and the precipitation efficiency remained consistently high, between 99.26% and 99.44%. This indicates that $Ni^{2+}$ ions were almost completely removed from the solution across the studied range. The results demonstrate that variations in the initial $[Ni^{2+}]_0$ concentration exerted little influence on the overall removal efficiency, provided that the pH was maintained under optimal conditions to ensure sufficient supersaturation for nucleation and crystal growth. This behavior suggests that the precipitation process is primarily governed by the supersaturation state of the system, which depends on the relative ion activity and pH, rather than the absolute $[Ni^{2+}]_0$ concentration. Previous studies have also reported that $Ni^{2+}$ precipitation efficiency can exceed 97–98% even at elevated concentrations when these parameters are properly controlled. For example, Salcedo *et al.* (2015) showed that the precipitation of $Ni^{2+}$ in a pellet reactor with initial concentrations between 200 and 300 mg $L^{-1}$ still achieved efficiencies above 97% under conditions of excess hydroxyl and optimal pH.[55] Similarly, Abdel-Aal (2000) demonstrated that increasing the initial $[Ni^{2+}]_0$ concentration during metal precipitation can affect the size and morphology of the precipitate particles, but did not reduce the removal efficiency as long as supersaturation was maintained.[56] Collectively, these findings confirm that the decisive factor for achieving high precipitation efficiency is not the absolute $[Ni^{2+}]_0$ concentration, but rather the maintenance of an appropriate anion/cation ratio and pH, which govern the supersaturation state and crystallization kinetics.

## 5. Characterization

The XRD pattern of the leached Ni-bearing wastewater sludge exhibits numerous well-defined reflections within $2\theta = 30–65°$, indicative of multiple oxide and spinel phases typical of metal-rich residues (Fig. 5a). Intense peaks at 36.7° and 43.3° are indexed to the (111) and (200) planes of NiO (JCPDS 47-1049), consistent with previously reported NiO patterns.[57] Additional reflections at about 35.6° and 57.0° correspond to the spinel structure of $NiFe_2O_4$, as commonly observed in Ni–Fe ferrites.[58] Secondary peaks between 33.5° and 36.5° match the characteristic reflections of $Cr_2O_3$,[59] while broad features in the ranges 24–33° and 49–64° indicate the presence of $Fe_2O_3$ (hematite), a frequent component of iron-rich sludge.[60] Weak peaks near 31–32° and 50–55° suggest contributions from $CaAl_2O_4$ and related aluminate phases, consistent with the initial Ca and Al content.[61] The presence of these oxide and spinel phases confirms that, although the leaching process effectively removed soluble and amorphous fractions, a portion of highly stable crystalline oxides such as NiO, $Fe_2O_3$, and $NiFe_2O_4$ remained in the residue. These species are chemically inert under ambient conditions, posing minimal environmental risk, and their persistence simply reflects the incomplete dissolution of refractory mineral phases rather than insufficient leaching efficiency. To further enhance metal recovery, additional treatments such as reductive leaching, sequential acid extraction, or mechanochemical activation could be employed to facilitate the dissolution of these refractory oxides. A macroscopic image of the green nickel precipitate obtained under optimal precipitation conditions is shown in Fig. S7, confirming the characteristic color of $Ni(OH)_2$ and NiOOH prior to further structural analyses.

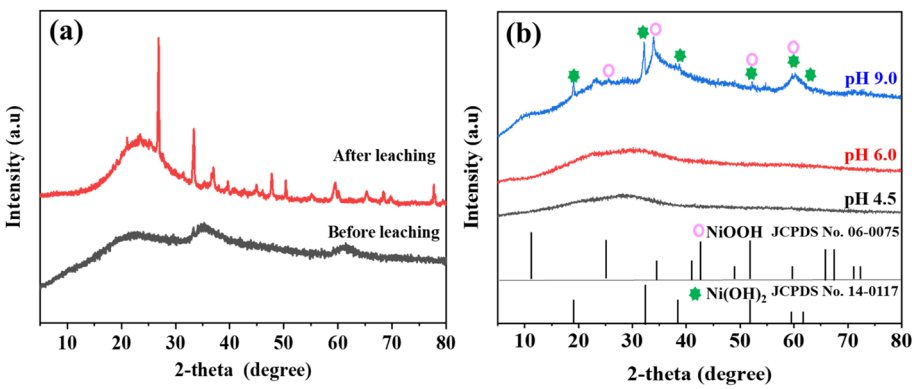


Fig. 5 XRD patterns of (a) Ni wastewater sludge samples before and after leaching, and (b) precipitated samples at pH 4.5, 6.0, and 9.0.

Meanwhile, the XRD analysis in Fig. 5(b) reveals the phase evolution of the mixed-metal precipitates obtained from the leachate. A clear transformation in phase composition and crystallinity is observed with increasing pH, confirming that a progressively alkaline environment strongly promotes the selective precipitation and structural ordering of metal hydroxides. At pH 4.5, the diffraction pattern displays a broad, featureless background without any distinct reflections, indicating that the solid phase mainly consists of amorphous ferric hydroxides formed through the rapid hydrolysis of $Fe^{3+}$. As the pH increases to 6.0, $Al^{3+}$ and $Cr^{3+}$ species begin to co-precipitate gradually as amorphous or poorly crystalline hydroxides, while $Ni^{2+}$ remains largely soluble. At pH 9.0, the pattern exhibits sharp and well-defined reflections, evidencing the dominant formation of crystalline β-$Ni(OH)_2$. The characteristic diffraction peaks located at approximately $2\theta \approx 19.05°$, 32.16°, 38.71°, 52.10°, 59.12°, and 62.12° correspond to the (001), (100), (101), (102), (110), and (111) planes, which can be indexed mainly to β-$Ni(OH)_2$ (JCPDS No. 14-0117),[62] with a minor contribution from the (100) reflection of α-$Ni(OH)_2$. Notably, the reflections at around 25°, 34.57°, 52.10° and 59.12° are also attributable to the characteristic planes of NiOOH (JCPDS No. 06-0075),[63] indicating the partial oxidation of $Ni(OH)_2$ into NiOOH during synthesis. These results collectively confirm that under strongly alkaline conditions (pH 9.0), nickel is selectively and efficiently precipitated as a mixture of highly crystalline β-$Ni(OH)_2$ and NiOOH phases, marking the complete conversion of soluble $Ni^{2+}$ into stable solid hydroxide/oxyhydroxide products.

The SEM-EDX results in Fig. 6(a–f) illustrate the morphological and compositional evolution of the Ni-bearing sludge throughout the sequential treatment stages. In the untreated sludge (Fig. 6(a and b)), the SEM micrograph reveals an amorphous, loosely aggregated surface composed of irregular clusters ranging from a few to several tens of micrometers. The particles exhibit rough textures, abundant voids, and indistinct boundaries, consistent with a heterogeneous mixture of metal hydroxides and poorly crystallized oxides typical of electroplating sludge. The corresponding EDX spectrum confirms

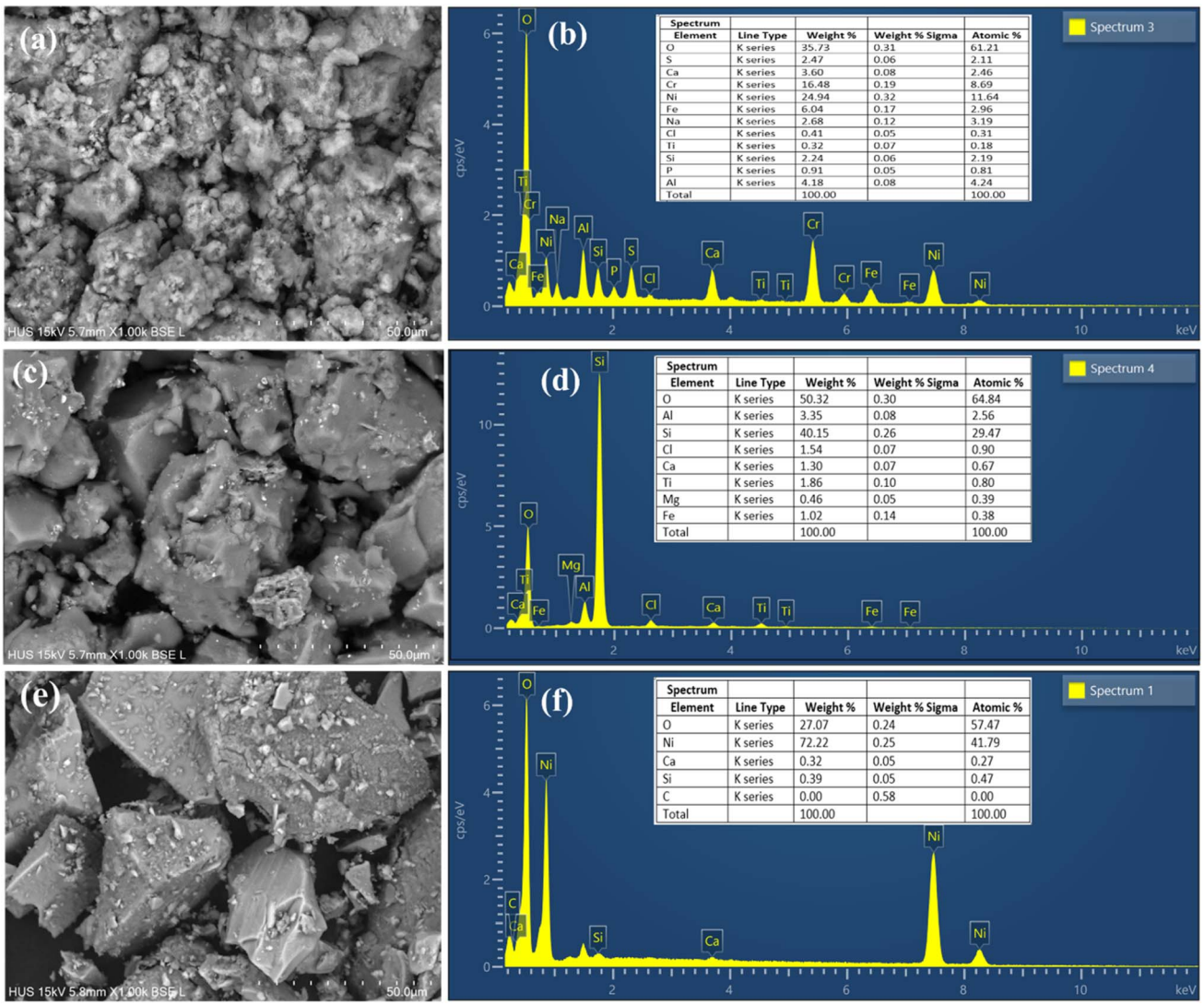


Fig. 6 SEM-EDX of Ni sludge samples (a and b) before, (c and d) after leaching, and (e and f) after precipitation at pH 9.0.

a polymetallic composition dominated by Ni (24.94 wt%), Cr (16.48 wt%), and Fe (6.04 wt%), together with Ca, Ti, Al, Na, and P as minor elements. The high O content (35.73 wt%) supports the presence of hydrated oxide and hydroxide phases. These features collectively indicate that the raw sludge matrix is chemically complex and structurally disordered, forming a porous amorphous aggregate.

After acid leaching (Fig. 6(c and d)), the surface morphology changes markedly. The residual solids appear denser and smoother, with flattened faces and sharp edges replacing the irregular aggregates. Occasional radial cracks and fracture planes suggest recrystallization and phase rearrangement during dissolution. The EDX spectrum shows a pronounced decrease in Ni, Cr, and Fe signals, confirming their effective extraction while O and Si become dominant, accounting for 50.32 wt% and 40.15 wt%, respectively. Increased Al and Mg contents further indicate that the residual solid primarily consists of silicate and aluminosilicate frameworks derived from inert supporting materials. The morphological densification and higher O/Si ratio are consistent with the XRD results showing sharper peaks and reduced metallic intensity after leaching, confirming the depletion of transition metals and the formation of a more ordered mineral matrix.

At the Ni precipitation stage (pH 9.0) (Fig. 6(e and f)), the morphology undergoes a pronounced transformation. Well-defined polyhedral and plate-like crystals with smooth facets and uniform sizes (tens of micrometers) are clearly visible, forming densely packed aggregates that differ substantially from both the amorphous raw sludge and the irregular leached residues. The corresponding EDX spectrum (Fig. 6(f)) confirms a strong Ni signal (72.22 wt%) together with O (27.07 wt%), while only trace levels of Si and Ca are detected, and no significant impurities such as Fe, Al, or Na are present. This composition demonstrates that nickel is the dominant constituent, and the Ni/O atomic ratio is consistent with the stoichiometry of nickel hydroxide or oxyhydroxide. The well-crystallized polyhedral morphology further supports the formation of β-$Ni(OH)_2$ and NiOOH as the major phases under the strongly alkaline and mildly oxidizing conditions at pH 9. These findings confirm that the precipitation stage effectively regenerated high-purity nickel hydroxide/oxyhydroxide products with a homogeneous crystalline framework and minimal contamination from other elements.

## 6. Preliminary cost analysis for 1 kg $Ni(OH)_2$/NiOOH recovered from electroplating sludge

Preliminary cost analysis indicates that producing 1 kg of $Ni(OH)_2$ or NiOOH from electroplating sludge *via* the leaching–precipitation process can be directly estimated based on experimental operating parameters (in Fig. S2). The amount of $H_2SO_4$ required to dissolve the corresponding Ni content is approximately 22–26 L of 5% $H_2SO_4$ solution, equivalent to a cost of 3.3–6.5 USD assuming bulk industrial acid pricing of 0.15–0.25 USD/L. The subsequent pH adjustment from 2 to 9 requires 2.0–2.3 kg of NaOH, corresponding to a cost of 2.0–3.5 USD based on industrial NaOH prices of 1.0–1.5 USD/kg. The electrical energy consumed for stirring, phase separation, and drying is estimated at 30–45 kWh, giving a cost of 3.6–6.8 USD assuming an industrial electricity price of 0.12–0.15 USD/kWh. The amount of Fe–Al–Cr sludge generated after precipitation is approximately 0.05–0.12 kg per kg of product. Using typical industrial hazardous-sludge treatment fees (which should be refined in actual operation), the estimated disposal cost is 0.8–2.4 USD. Depreciation, maintenance, and operation of corrosion-resistant equipment (HDPE/FRP tanks, PVC-U pipelines, acid–base metering pumps) contribute an additional 1.0–1.5 USD/kg. Summing all contributions, the total production cost of 1 kg of $Ni(OH)_2$ or NiOOH is estimated at 10.7–20.7 USD/kg. When compared with typical commercial market prices ($Ni(OH)_2$ : 28–40 USD/kg, NiOOH: 30–45 USD/kg), the resulting expected profit margin of ~15–25 USD/kg demonstrates the strong economic feasibility of converting electroplating sludge into high-value $Ni(OH)_2$/NiOOH products.

## 7. Current challenges and future prospects

Although Ni recovery from electroplating sludge *via* the metal leaching–precipitation route has proven efficient, environmentally benign, and promising for practical implementation, several challenges remain before large-scale deployment. The intrinsic heterogeneity of real electroplating sludge presents a major obstacle. The metal composition, water content, particle size, and impurity levels vary significantly among different facilities, making it difficult to standardize treatment protocols. This necessitates comprehensive material characterization and adaptable process tuning to ensure consistent performance under variable conditions. In addition, selectivity in the leaching–precipitation step still requires further optimization. While dilute $H_2SO_4$ effectively suppresses Fe and Al dissolution, co-precipitation or secondary phase formation between Ni and other cations may compromise product purity. Detailed investigations into reaction mechanisms, crystallization kinetics, and the role of competing ions could improve both selectivity and the simultaneous recovery of valuable metals such as Cu, Zn, and Co. What's more, scaling and economic feasibility must be critically assessed. At laboratory scale, reagent consumption and energy demand are easily managed, but industrial operation introduces challenges related to process economics, equipment corrosion, and secondary sludge management. Integrating Ni recovery into existing wastewater treatment lines or applying continuous systems such as fluidized bed reactors could enhance efficiency and cost-effectiveness. Finally, from a sustainability standpoint, valorizing the recovered NiOOH and β-$Ni(OH)_2$ precipitate represents a promising pathway toward circular resource utilization. The β-$Ni(OH)_2$ phase obtained in this study is not merely a secondary by-product but a technologically valuable material. Benefiting from its high theoretical capacity, reversible $Ni^{2+}$/$Ni^{3+}$ redox behavior, and outstanding chemical stability,

$Ni(OH)_2$ has been extensively applied in nickel-based batteries (Ni–Cd and Ni–MH), supercapacitors, electrochemical sensors, and as a precursor for NiO or NiOOH catalysts in energy conversion and storage systems. For instance, $Ni(OH)_2$/XC-72 composite exhibits specific capacitance ~1296 F $g^{-1}$ in supercapacitor tests.[64] Furthermore, a $Ni(OH)_2$/Co–C–N composite achieved up to ~2100 F $g^{-1}$ and outstanding cycling stability (90.2% after 5000 cycles) for flexible supercapacitors.[65]

The NiOOH phase, which is generated from $Ni(OH)_2$ through electrochemical oxidation during battery or supercapacitor operation, represents another high-value functional material. NiOOH serves as the primary redox-active species at the positive electrode in Ni–MH batteries and has been extensively studied for its excellent reversibility and high specific capacity.[66] Recent developments in asymmetric supercapacitors employing NiOOH-based electrodes have reported notable energy densities, reaching approximately 0.4 mWh $cm^{-2}$, underscoring its strong charge storage capability.[67] Furthermore, NiOOH and its derivatives have demonstrated exceptional catalytic activity toward the oxygen evolution reaction (OER) in alkaline electrolytes.[68] For example, NiOOH thin films exhibit efficient water oxidation performance, making them promising candidates for energy conversion and storage technologies.[69] Therefore, converting electroplating sludge into $Ni(OH)_2$ (and potentially NiOOH *via* further electrochemical activation) not only alleviates environmental concerns but also establishes a sustainable route for producing functional materials with significant potential in electrochemical and catalytic applications. Although the electrochemical properties and catalytic activity of $Ni(OH)_2$/NiOOH have been widely established in previous studies, a direct assessment of the $Ni(OH)_2$ materials synthesized in this work such as their charge-storage behavior, redox characteristics, and OER catalytic performance remains essential. Such evaluations will serve as a key future research direction to validate their application potential and further optimize product utilization within a circular-economy framework. In this context, combining Life Cycle Assessment (LCA) with Techno-Economic and Environmental Assessment (TEA) will be essential to evaluate the overall feasibility and guide commercialization strategies.

## 8. Conclusion

This study reports the successful development of an integrated process combining dilute acid leaching and metal precipitation for nickel recovery from real electroplating sludge. The method is distinguished by the use of a low-concentration, moderate-temperature acid leach followed by a precisely controlled hydroxide precipitation step. This combination is well-suited to industrial sludge treatment and helps minimize chemical consumption, equipment corrosion, and secondary pollution while maintaining high efficiency and environmental compatibility. Systematic optimization defined practical operating conditions for industrial applications. In the leaching stage, nickel was almost completely extracted (99.70%) under mild conditions using 5% $H_2SO_4$ at a 1 : 10 S/L ratio, 55 °C, and 40 min, while dissolution of iron and other metals was effectively suppressed. Subsequent precipitation with NaOH achieved recovery efficiencies above 98% at pH 9, and an initial $[Ni^{2+}]_0$ concentration of 2000 mg $L^{-1}$, ensuring efficient hydroxyl use and high product purity. XRD confirmed that the precipitate consisted primarily of highly crystalline NiOOH and $Ni(OH)_2$, SEM revealed uniform polyhedral crystals, and EDX analysis verified nickel as the dominant element with minimal impurities. These results demonstrate not only the effective recovery of valuable nickel resources but also a substantial reduction of the environmental risks associated with electroplating sludge. The integrated process therefore provides an economical, sustainable, and readily deployable solution for small- and medium-scale production facilities, offering a practical model for circular metal recycling within the electroplating industry and related sectors.

## Conflicts of interest

The authors declare that they have no known competing financial interests or personal relationships that could have appeared to influence the work reported in this paper.

## Data availability

Data will be provided to the extent necessary upon request.

Supplementary information (SI): additional figures, tables, and experimental details supporting the findings of the main manuscript, including extended material characterization, adsorption isotherm fitting parameters, kinetic model data, and supplementary control experiments. See DOI: https://doi.org/10.1039/d5ra08573j.

## Acknowledgements

This research was funded by the research project QG.23.78 of Vietnam National University, Hanoi.

## References

1 R. Huang, K.-L. Huang, Z.-Y. Lin, J.-W. Wang, C. Lin and Y.-M. Kuo, Recovery of valuable metals from electroplating sludge with reducing additives *via* vitrification, *J. Environ. Manage.*, 2013, **129**, 586–592.

2 T. Scarazzato, Z. Panossian, J. A. S. Tenório, V. Pérez-Herranz and D. C. R. Espinosa, A review of cleaner production in electroplating industries using electrodialysis, *J. Cleaner Prod.*, 2017, **168**, 1590–1602.

3 C. Li, F. Xie, Y. Ma, T. Cai, H. Li, Z. Huang and G. Yuan, Multiple heavy metals extraction and recovery from hazardous electroplating sludge waste *via* ultrasonically enhanced two-stage acid leaching, *J. Hazard. Mater.*, 2010, **178**, 823–833.

4 Z. Suiyi, L. Xin, Z. Minglin, L. Yingzi, L. Siwen, H. O. Kaung, Y. Weilu, Q. Wensheng, J. Temuujin, Y. Yang, L. Jiancong, L. Wenjing and C. Yu, Hydrometallurgy recycling of heavy metals from electroplating sludge: Recent development and challenge, *Chem. Eng. Res. Des.*, 2025, **214**, 269–280.

5 D. C. R. Espinosa and J. A. S. Tenório, Thermal behavior of chromium electroplating sludge, *Waste Manage.*, 2001, **21**, 405–410.
6 C. J. Smith, P. Hopmans and F. J. Cook, Accumulation of Cr, Pb, Cu, Ni, Zn and Cd in soil following irrigation with treated urban effluent in Australia, *Environ. Pollut.*, 1996, **94**, 317–323.
7 M. J. McLaughlin, B. A. Zarcinas, D. P. Stevens and N. Cook, Soil testing for heavy metals, *Commun. Soil Sci. Plant Anal.*, 2000, **31**, 1661–1700.
8 L. Mao, R. Tang, Y. Wang, Y. Guo, P. Su and W. Zhang, Stabilization of electroplating sludge with iron sludge by thermal treatment *via* incorporating heavy metals into spinel phase, *J. Cleaner Prod.*, 2018, **187**, 616–624.
9 Y. Zhou, Z. Zhang, L. Zhang, S. Xu, B. Guo, Y. Liu and S. Xia, Promoting waste activated sludge reduction by linear alkylbenzene sulfonates: Surfactant dose control extracellular polymeric substances solubilization and microbial community succession, *J. Hazard. Mater.*, 2019, **374**, 74–82.
10 R. G. McDonald and B. I. Whittington, Atmospheric acid leaching of nickel laterites review: Part I. Sulphuric acid technologies, *Hydrometallurgy*, 2008, **91**, 35–55.
11 S. Donatello and C. R. Cheeseman, Recycling and recovery routes for incinerated sewage sludge ash (ISSA): A review, *Waste Manage.*, 2013, **33**, 2328–2340.
12 P. T. Huyen, T. D. Dang, M. T. Tung, N. T. T. Huyen, T. A. Green and S. Roy, Electrochemical copper recovery from galvanic sludge, *Hydrometallurgy*, 2016, **164**, 295–303.
13 M. Oncel, A. Muhcu, E. Demirbas and M. Kobya, A comparative study of chemical precipitation and electrocoagulation for treatment of coal acid drainage wastewater, *J. Environ. Chem. Eng.*, 2013, **1**, 989–995.
14 A. H. Kaksonen, S. Särkijärvi, J. A. Puhakka, E. Peuraniemi, S. Junnikkala and O. H. Tuovinen, Solid phase changes in chemically and biologically leached copper smelter slag, *Miner. Eng.*, 2017, **106**, 97–101.
15 L. Twidwell, D. Dahnke, B. Arthur and S. Nordwick, Recovery of metal values from metal finishing hydroxides sludges by phosphate precipitation, in: Land disposal, remedial action, incineration and treatment of hazardous waste. *Proceedings of the 12 Th Annual Research Symposium*, Cincinnati, Ohio, United States, 1986, pp. 338–351.
16 G.-B. Liu, C.-H. Wei, T. Liu, H.-Y. Luo, H. Zhou, H.-W. Rong, D. Chen and H. H. Ngo, Electroplating wastewater treatment and resource recovery *via* a hybrid process of stepwise alkalization, Fenton, and chlorination, *Sep. Purif. Technol.*, 2024, **339**, 126658.
17 A. Chernyaev, B. P. Wilson and M. Lundström, Study on valuable metal incorporation in the Fe–Al precipitate during neutralization of LIB leach solution, *Sci. Rep.*, 2021, **11**, 23283.
18 H. F. Scott, *Elements of Chemical Reaction Engineering*, Prentice Hall, 2016.
19 J. B. Jensen, V. Kueeš and M. Kubal, Electrokinetic remediation of soils polluted with heavy metals. Removal of zinc and copper using a new concept, *Environ. Technol.*, 1994, **15**, 1077–1082.
20 X. Zhang, G. Li, J. Wu, N. Xiong and X. Quan, Leaching of Valuable Elements from the Waste Chromite Ore Processing Residue: A Kinetic Analysis, *ACS Omega*, 2020, **5**, 19633–19638.
21 P. K. Parhi, K. H. Park and G. Senanayake, A kinetic study on hydrochloric acid leaching of nickel from Ni–$Al_2O_3$ spent catalyst, *J. Ind. Eng. Chem.*, 2013, **19**, 589–594.
22 J. Cui, N. Zhu, D. Luo, Y. Li, P. Wu, Z. Dang and X. Hu, The Role of Oxalic Acid in the Leaching System for Recovering Indium from Waste Liquid Crystal Display Panels, *ACS Sustain. Chem. Eng.*, 2019, **7**, 3849–3857.
23 B. Pospiech and M. Warzecha, Application of oxalic acid as an efficient leaching agent of aluminum from industrial waste, *Physicochem. Probl. Miner. Process*, 2020, **56**, 264–270.
24 R. A. Hernández-Hernández, F. Legorreta-García, L. E. Hernández-Cruz, E. A. Chavez-Urbiola and E. Salinas-Rodríguez, Kinetics of Iron Leaching from Kaolinitic Clay, Using Phosphoric Acid, *Minerals*, 2016, **6**, 60.
25 I. Ali, A. Gaydukova, T. Kon'kova, Z. A. ALOthman and M. Sillanpää, Kinetics and Optimization of Metal Leaching from Heat-Resistant Nickel Alloy Solid Wastes, *Molecules*, 2023, **28**, 5545.
26 V. Gunarathne, A. U. Rajapaksha, M. Vithanage, D. S. Alessi, R. Selvasembian, M. Naushad, S. You, P. Oleszczuk and Y. S. Ok, Hydrometallurgical processes for heavy metals recovery from industrial sludges, *Crit. Rev. Environ. Sci. Technol.*, 2022, **52**, 1022–1062.
27 T. Xu, Y. Xu, N. Liao, Y. Li and M. Nath, High-Temperature Chemical Stability of Cr(III) Oxide Refractories in the Presence of Calcium Aluminate Cement, *Materials*, 2021, **14**(21), 6590.
28 S. Shukla, A. Chernyaev, P. Halli, J. Aromaa and M. Lundström, Leaching of Waste Pharmaceutical Blister Package Aluminium in Sulphuric Acid Media, *Metals*, 2023, **13**, 1118.
29 M. K. Jha, V. Kumar and R. J. Singh, Review of hydrometallurgical recovery of zinc from industrial wastes, *Resour., Conserv. Recycl.*, 2001, **33**, 1–22.
30 M. S. W. Lim, T. C. K. Yang, Y. H. Yap, G.-T. Pan, S. Chong and T. J. Tiong, Intensification and optimisation of nickel recovery from spent hydrogenation catalysts *via* ultrasound-augmented hydrometallurgy, *J. Environ. Chem. Eng.*, 2021, **9**, 105771.
31 H. M. Santos, C. Lodeiro and J.-L. Capelo-Martinez, The power of ultrasound, *UCA*, 2009, 1–16.
32 T. A. Kurniawan, G. Y. S. Chan, W.-H. Lo and S. Babel, Physico–chemical treatment techniques for wastewater laden with heavy metals, *Chem. Eng. J.*, 2006, **118**, 83–98.
33 F. Faraji, A. Alizadeh, F. Rashchi and N. Mostoufi, Kinetics of leaching: a review, *Rev. Chem. Eng.*, 2022, **38**, 113–148.
34 R. Salhi, M. Boudjouada, S. Messikh and N. Gherraf, Recovery of nickel and copper from metal finishing hydroxide sludge by kinetic acid leaching, *J. New Technol. Mater.*, 2016, **6**, 62–71.

35 S. Top, S. Kursunoglu and Z. T. Ichlas, Effects of leaching parameters on the dissolution of nickel, cobalt, manganese and iron from Caldag lateritic nickel ore in hydrochloric acid solution, *Can. Metall. Q.*, 2020, **59**, 368–376.
36 A. H. Ibrahim, X. Lyu, B. M. Atia, M. A. Gado and A. B. ElDeeb, Cost-Effective and High Purity Valuable Metals Extraction from Water Leaching Solid Residues Obtained as a By-Product from Processing the Egyptian Boiler Ash, *Minerals*, 2022, **12**, 1084.
37 G. Prameswara, F. Y. P. Tyassena, M. Pasaribu, I. Trisnawati and H. T. B. M. Petrus, Nickel Recovery Optimization and Kinetic Study of Morowali Laterite Ore, *Trans. Indian Inst. Met.*, 2023, **76**, 1341–1348.
38 X. Bu, Z. Tong, M. Bilal, X. Ren, M. Ni, C. Ni and G. Xie, Effect of ultrasound power on HCl leaching kinetics of impurity removal of aphanitic graphite, *Ultrason. Sonochem.*, 2023, **95**, 106415.
39 Y. Lin, H. Sun, T. Peng, D. Zhao and X. Zhang, The Leaching Kinetics of Iron from Titanium Gypsum in a Citric Acid Medium and Obtain Materials by Leaching Liquid, *Molecules*, 2023, **28**(3), 952.
40 E. Kuzas, I. Sandalov, K. Karimov, A. Kritskii, I. Fomenko, I. Zhidkov and A. Abramov, Kinetics of Iron Collector Leaching in HCl and HF Media, *Metals*, 2024, **14**, 1077.
41 X. Li, Z. Peng and Y. Yang, Leaching Kinetics and Reactive Regulation of Boiling Furnace Pyrite Cinder (BPC) in an Oxalic Acid-Sulfuric Acid System, *Processes*, 2025, **13**, 2904.
42 D. Daminescu, N. Duteanu, M. Ciopec, A. Negrea, P. Negrea, N. S. Nemeș, B. Pascu, R. Lazău and A. Berbecea, Kinetic Modelling the Solid–Liquid Extraction Process of Scandium from Red Mud: Influence of Acid Composition, Contact Time and Temperature, *Materials*, 2023, **16**, 6998.
43 X. Liu, H. Xu, Z. Zhao, Y. Ma, J. Zhang, Q. Li, X. Chen, J. Li, X. Zhao, L. He, Y. Li, W. Zhang, F. Sun and J. Guo, Kinetics of Nickel Leaching from Middling Nickel Matte with Sulfuric Acid Under Atmospheric Pressure, *J Sustain Metall.*, 2025, **11**, 4311–4321.
44 Z. Guo, P. Guo, G. Su and F. Li, Study on Ultrasonically-Enhanced Sulfuric Acid Leaching of Nickel from Nickel-Containing Residue, *Crystals*, 2021, **11**, 810.
45 C. Pan, H. Liu, J. G. Catalano, Z. Wang, A. Qian and D. E. Giammar, Understanding the Roles of Dissolution and Diffusion in $Cr(OH)_3$ Oxidation by δ-$MnO_2$, *ACS Earth Space Chem.*, 2019, **3**, 357–365.
46 P. W. Atkins, J. De Paula, J. Keeler, *Atkins' Physical Chemistry*, Oxford university press, 2023.
47 O. Levenspiel, *Chemical Reaction Engineering*, John wiley & sons, 1998.
48 Z. Xu, Y. Wang, B. Zhu, G. Wei, F. Ma, Z. Yu and J. Qu, Microbubble Oxidation for $Fe^{2+}$ Removal from Hydrochloric Acid Laterite Ore Leachate, *Materials*, 2023, **16**, 6951.
49 S. Hidayat, S. Yulianti, D. Anggreini and S. Bahtiar, Study of Nickel Leaching Using Sulfuric Acid and Phosphoric Acid on The Selectivity Nickel Ore, *Pijar Mipa*, 2021, **16**, 393–396.
50 X. Zhao, S. Qiang, H. Wu, Y. Yang, D. Shao, L. Fang, J. Liang, P. Li and Q. Fan, Exploring the Sorption Mechanism of Ni(II) on Illite: Batch Sorption, Modelling, EXAFS and Extraction Investigations, *Sci. Rep.*, 2017, **7**, 8495.
51 M. Z. Mubarok and J. Lieberto, Precipitation of Nickel Hydroxide from Simulated and Atmospheric-leach Solution of Nickel Laterite Ore, *Procedia Earth Planet. Sci.*, 2013, **6**, 457–464.
52 C. Sist and G. P. Demopoulos, Nickel hydroxide precipitation from aqueous sulfate media, *JOM*, 2003, **55**, 42–46.
53 B. Mavis, *Homogeneous Precipitation of Nickel Hydroxide Powders*, Iowa State University, 2003.
54 Y. Shekarian, M. Rezaee and S. Pisupati, Green chemical precipitation of manganese, cobalt, and nickel from acid mine drainage using ozone: mechanism and chemical kinetics, *React. Chem. Eng.*, 2025, **10**(10), 2398–2411.
55 A. Salcedo, F. Ballesteros and M. Lu, Recovery of nickel from industrial wastewater by homogeneous fluidized-bed granulation: effects of influent nickel concentration, CO3: Ni ratio and pH of the precipitant, in *Proceedings of the 14th International Conference on Environmental Science and Technology*, 2015, pp. 1–5.
56 E. A. Abdel-Aal and M. M. Rashad, Kinetic study on the leaching of spent nickel oxide catalyst with sulfuric acid, *Hydrometallurgy*, 2004, **74**, 189–194.
57 H. Yan, D. Zhang, J. Xu, Y. Lu, Y. Liu, K. Qiu, Y. Zhang and Y. Luo, Solution growth of NiO nanosheets supported on Ni foam as high-performance electrodes for supercapacitors, *Nanoscale Res. Lett.*, 2014, **9**, 424.
58 T. M. Naidu and P. L. Narayana, Technology, Synthesis and characterization of Fe-$TiO_2$ and $NiFe_2O_4$ nanoparticles and its thermal properties, *J Nanosci Technol.*, 2019, 769–772.
59 X. Xu, J. Wu, N. Yang, H. Na, L. Li and J. Gao, $Cr_2O_3$: a novel supercapacitor electrode material with high capacitive performance, *Mater. Lett.*, 2015, **142**, 172–175.
60 D. E. Fouad, C. Zhang, H. El-Didamony, L. Yingnan, T. D. Mekuria and A. H. Shah, Improved size, morphology and crystallinity of hematite (α-$Fe_2O_3$) nanoparticles synthesized *via* the precipitation route using ferric sulfate precursor, *Results Phys.*, 2019, **12**, 1253–1261.
61 C. Bhavya, K. Yogendra and K. Mahadevan, Synthesis of Calcium aluminate nanoparticle and its application to photocatalytic degradation of Coralene Navy Blue 3G and Coralene Violet 3R, *Int. J. Res. Chem. Environ.*, 2015, **5**(1), 28–33.
62 Y. Qu, W. Zhou, X. Miao, Y. Li, L. Jiang, K. Pan, G. Tian, Z. Ren, G. Wang and H. Fu, A New Layered Photocathode with Porous NiO Nanosheets: An Effective Candidate for p-Type Dye-Sensitized Solar Cells, *Chem.–Asian J.*, 2013, **8**, 3085–3090.
63 R. Thimmasandra Narayan, Effect of Crystallinity of β-and βbc-Nickel Hydroxide Samples on Chemical Cycling, *Indian J. Eng. Mater. Sci.*, 2015, **2015**, 820193.
64 S. Tang, L. Sui, Z. Dai, Z. Zhu and H. Huangfu, High supercapacitive performance of $Ni(OH)_2$/XC-72 composite prepared by microwave-assisted method, *RSC Adv.*, 2015, **5**, 43164–43171.
65 D. Li, C. Shen, Q. Lu, R. Yan, B. Xiao, B. Zi, J. Zhang, Q. Lu and Q. Liu, Excellent performance supercapacitors with

the compounding of $Ni(OH)_2$ and ZIF-67 derived Co–C–N nanosheets as flexible electrode materials, *Nanoscale Adv.*, 2022, **4**, 4381–4390.

66 X. Yi, C. Kirk and N. Robertson, Nickel hydroxide-based energy storage devices: nickel-metal hydride batteries *vs.* nickel hydroxide hybrid supercapacitors, *Carbon Neutrality*, 2024, **3**, 39.

67 T. Zhou, Z. Qiu, C. Hao, Q. Gao, Y. Zhao, J. Zhao, L. Jing, J. Lv, H. Li and J. Zhao, Enhanced asymmetric supercapacitor performance of NiOOH electrodes from hexagonal $Ni(OH)_2$ nanosheets *via* low-concentration $OH^-$-mediated growth and galvanostatic oxidation, *J. Energy Storage*, 2025, **137**, 118558.

68 O. Diaz-Morales, D. Ferrus-Suspedra and M. T. M. Koper, The importance of nickel oxyhydroxide deprotonation on its activity towards electrochemical water oxidation, *Chem. Sci.*, 2016, **7**, 2639–2645.

69 R. P. Putra, I. B. Rachman, H. Horino and I. I. Rzeznicka, Bifunctional Catalytic Activity of γ-NiOOH toward Oxygen Reduction and Oxygen Evolution Reactions in Alkaline Solutions, *Oxygen*, 2022, **2**, 479–492.